Journal of Applied Polymer Science

Poly Lactic Acid Nanocomposites Containing Modified Nanoclay with Synergistic Barrier to Water Vapor for Coated Paper

M. Farmahini-Farahani,[1] Huining Xiao,[1,2] Yi Zhao[2]

[1]Department of Chemical Engineering and Limerick Pulp & Paper Centre, University of New Brunswick, Fredericton NB E3B 5A3, Canada

[2]School of Environmental Science & Engineering, North China Electric Power University, Baoding 071003, China

Correspondence to: H. Xiao (E-mail: hxiao@unb.ca)

ABSTRACT: The binary nanocomposites of poly lactic acid (PLA) with the montmorillonite modified with trisilanol polyhedral oligomeric silsesquioxanes (Trisilanolisooctyl POSS®) were prepared via a solution-blending process and coated on paper by bar coating and compress hot melt coating methods. The resulting components were characterized with Fourier transform infrared spectroscopy, and X-ray diffraction (XRD) techniques. Moreover, the water vapor transmission rates (WVTR) for the coated writing paper were determined using an IGA-003. The results indicated that the modified clay PLA nanocomposites enhanced the water vapor barrier properties of coated paper significantly. The permeability of PLA nanocomposites to water vapor decreased by 74% [26.0 g/(m^2 day)], respectively, as compared to those of the paper coated with pure PLA. The dispersion and phase behavior of the modified montmorillonite in PLA matrix was revealed by Transmission electron microscope. The intercalation of montmorillonite with PLA was further demonstrated using XRD. WVTR results indicated that the compress hot melt coating of the nanocomposites is an effective method to improve the water vapor resistance of coated paper. © 2014 Wiley Periodicals, Inc. J. Appl. Polym. Sci. **2014**, *131*, 40952.

KEYWORDS: clay; coatings; nonpolymeric materials and composites

Received 29 August 2013; accepted 4 May 2014

DOI: 10.1002/app.40952

INTRODUCTION

Paper and paperboard are the only renewable materials widely used in packaging applications.[1–4] However, the hygroscopic and porous nature of paper limits its potential when shelf life concerns are taken into account.[5,6] Paper and paperboard intended for packaging materials are often coated with fossil-based and nonbiodegradable polymers, such as PE,[7,8] HDPE,[9] and, PP[10] with high barrier properties whose impact on the environment is under debate. Food packaging represents a high volume commodity with the use of paperboard-based products for shipping and handling purposes. Therefore, with the growing awareness of sustainability the focus on developing coated paper for food packaging has shifted from conventional plastic materials to more environmentally friendly alternatives, biodegradable coatings in particular.

Poly lactic acid (PLA) synthesized from renewable resources has attracted much attention, as it can achieve excellent mechanical properties at a competitive cost as a sustainable replacement for traditional petrochemical-derived polymers in packaging and paper coating applications.[11] PLA shows a limitation for the application of gas barrier to be used for food packaging, and it also has relatively low resistance to water vapor permeation compared with conventional fuel-based polymers.[12,13] Therefore, much work has been performed to improve the gas and water vapor permeation resistance of PLA.[13,14]

Blending polymers with additives such as nano-clays, nano-particles, and other polymers is a common and cost-effective approach to render materials with desired properties.[15,16] Biopolymer/clay nanocomposites have a wide range of potential applications.[17,18] Recently the research on improving vapor barrier properties by using a small amount of clay with a high aspect ratio and nanoparticles in polymer composites has drawn tremendous interest for packaging and paper coating applications.[19,20] Clay nanoparticles, montmorillonite (MMT) nanoclay in particular, can reduce oxygen, CO_2, and water vapor diffusion by creating a complex network in the biopolymer matrix.[20] The presence of fully exfoliated and dispersed silicate clay layers and nanoparticles creates a complex tortuous path for vapor molecules moving through the biopolymer matrix.[20] Exfoliated and intercalated silicate clay layers creates a large diffusion length and lowers the permeability, allowing biopolymer/clay nanocomposites to use in the packaging of foods and beverages, thus prolonging the shelf time as well as the freshness of the foods.[21] MMT/biopolymer nanocomposites display significant

improvements in mechanical, thermal properties, thermal stability, and enhances the retardation of oxygen and CO_2 diffusion. [20] MMT nanoclays also improve the water vapor transimisson rate.[18–21] AS MMT is hydrophilic naturally, it is necessary to modify MMT with hydrophobic chemicals in order to increase its compatibility with most hydrophobic polymer matrices and expand the interlayer space. This process allows large polymer molecules to enter between the clay plates for greater dispersion of organoclay to achieve a homogeneous nanocomposite.

Polyhedral oligomeric silsesquioxane (POSS), one of the smallest silica particles (1–3 nm), is well-known commercially.[22,23] POSS consists of a silica cage in the core with organic substituents R attached at the edges of the cage. By the variation of R group it could be a novel amphiphilic chemical structure and reveal extraordinary chemical, thermal, and mechanical properties.[23–25] Thus, POSS has not only been used for practical applications such as moisture sensitive shape memory,[26] compatibilizer,[27] clay modification and promoting melt-crystallization,[28] barrier properties improvement,[29–31] and coatings and membrane technology,[31,32] but also as a powerful tool for the characterization of hydrophobic and hydrophilic polymer nano-based composites.[33,34]

The objective of this work was to explore a novel modified MMT as a disperse phase for PLA nanocomposites, which were applied to the paper surface via two different coating processes in an attempt to lower the water vapor transfer resistance of the coated paper by a biodegradable polymer.

EXPERIMENTAL

Materials

The PLA used in experiments was Ingeo 2003D, purchased from NatureWorks, which has a $\bar{M}w = 193{,}000$ g mol^{-1} and $\bar{M}n = 114{,}000$ g mol^{-1} as determined by gel permeation chromatography (GPC). The PLA was purified by dissolution in anhydrous, chloroform (≥99%), and then precipitated in anhydrous methanol (99.8%) and dried under vacuum (20 inHg) overnight at 40°C prior to GPC measurements. Paper was selected from a commercial writing/printing paper (W&P paper) with 75 g/m^2, manufactured by Domtar. Organo-modified MMT, Cloisite® 30B, with bis-(2-hydroxyethyl) methyl (hydrogenated tallow alkyl) ammonium counter ions, was kindly donated by Southern Clay Products (Gonzalez, TX). The organic content of the organo-modified MMT, determined by Thermogravimetric Analysis (TGA), was 22 wt %. Prior to use, the clay was dried under vacuum at 110°C for 1 h. Trisilanolisooctyl Trisilanolisooctyl POSS® (98.2%) were purchased from Hybrid Plastics. Isophorone diisocyanate (IPDI 98%), anhydrous Tetrahydrofuran (THF), anhydrous Chloroform, anhydrous methanol, and dibutyltin dilaurate (DBTDL) catalyst were obtained from Sigma Aldrich and used without further purification. All powder materials were dried under vacuum (20 inHg) overnight at 40°C before use.

Characterization

Fourier Transform Infrared. Spectra were recorded to identify the chemical structure of the Cloisite 30B modified with trisilanolisooctyl POSS using a Perkin Elmer Spectrum 100 FT-IR Spectrometer.

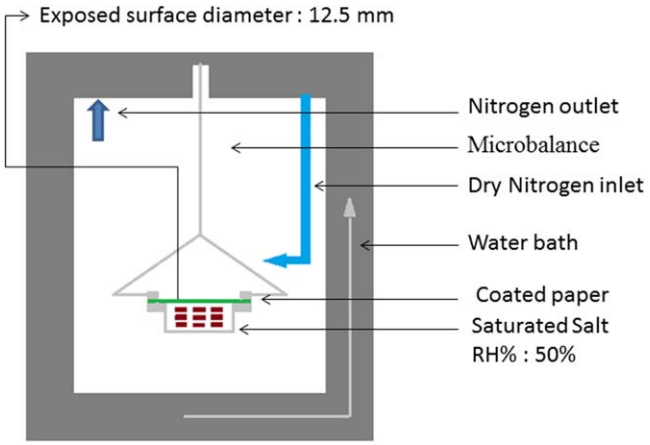

Scheme 1. Schematic illustration of IGA setup for WVTR testing. [Color figure can be viewed in the online issue, which is available at wileyonlinelibrary.com.]

X-ray Diffraction. The powder diffraction patterns of samples were collected on Bruker AXS D8 Advance solid-state powder diffraction X-ray diffraction (XRD) system with Cu$K\alpha$ radiation. The d-spacing of the intercalated clays and nanocomposites were determined by fitting Bragg's equation ($n\lambda = 2d\sin\theta$) in the range of 2–12 degrees (2θ) at a scan rate of 10 min^{-1}.

Thermogravimetric Analysis (TGA). The tests were carried out using a thermo-gravimetric analysis instrument (TA Instruments SDT Q600) in a temperature range of ambient to 600°C at a rate of 15 K/min^{-1} under the flow of N_2 with a flow rate of 100 mL/min^{-1}. The data obtained from the TGA instrument were in the form of weight percentage versus temperature.

Transmission Electron Microscope. Transmission electron microscopy (TEM) analysis was examined using a JEOL 2011 STEM. Molded nanocomposites by hot press were first trimmed with iron knives. Subsequently, the ultrathin sections were microtomed from these faces with a diamond knife. The microtomed sections were collected in a water-filled boat, which was operated at an accelerating voltage of 200 keV.

Water Vapor and Gas Transmission Rates. Measurements water vapor transmission rates (WVTR) of all coated paper samples were performed on IGA-003 (Hiden-Isochema, Warrington, UK) which consists of a high sensitivity microbalance (0.1 μg) and a turbomolecular high vacuum pumping system (see Scheme 1), in accordance to the methods described in TAPPI standard T464 om-12 (2012) and ASTM E96/E96M-05 (2005). In this experiment, coated paper samples (coating thickness 25 μm) was pre-conditioned on WVTR test measurement conditions for 72 hours to reach water adsorption equilibrium. The round coated paper samples were clamped in a permeation cell which was tight-ened by six screws. The measurements were carried out at 50% of the relative humidity (ΔRH%), which was achieved by saturated magnesium nitrate salt and flowing dry nitrogen gas at a flow rate of 20 mL/min. After the permeation cell was placed in a chamber, the data was collected after 1

h to allow the transmission to reach a steady state. The chamber temperature was controlled at 23°C. The weight reduction of the container, because of the moisture transfer, is proportional to the testing time. At constant temperature and ΔRH (%), WVTR can be calculated from the change in the weight of the container, at a specified time interval, and the area of exposed coated paper, as described by the following equation:

$$\text{WVTR} = \frac{\text{Weight Change}}{\text{Area} \times \text{time}} \quad (1)$$

Preparation of the Surface Modified Clays

Six g of Cloisite®30B (CS30B), which contains approximately 7.1 mmol hydroxyl groups, and 1.2 g of trisilanolisooctyl POSS® were added in THF (100 mL) in a 250 mL of three-necked, round-bottom flask equipped with a magnetic stirrer, nitrogen inlet, thermometer, and condenser with a drying tube. The suspension was then heated up to 50°C, and two drops of dibutyltin dilaurate (DBTDL) were added. Then IPDI (0.2 mL) drop wise was added and the reaction continued for 5 h. Excess ethylene glycol (0.2 g) was added to the mixture to react with the remaining IPDI for 1 h and cooled down to 0°C. The mixture was filtered, washed three times with chloroform, subsequently washed three times with deionized water, and then dried overnight in a vacuum oven at room temperature.

Preparation of PLA/MMT Nanocomposites

The PLA nanocomposites were prepared through a solution method with the addition of 5 and 10 wt % of Cloisite® 30B (CS30B) and 1, 3, 5, and, 10 wt % surface modified Cloisite® 30B (M-CS30B). For the fabrication of the nanocomposites, the following process was employed: First, appropriate amounts of PLA and clay were dissolved separately in chloroform. Then, the PLA solution and the clay solution were mixed together and stirred with sonication for 1 h. Nanocomposites powder was prepared by precipitation of the solution into an excess of methanol, and then the filtering process was followed. Finally, the end products were dried at 70°C under vacuum for 3 days to remove the solvent completely.

Paper Coating

The solution bar coating and compress hot melt coating methods were used to coat PLA and PLA nanocomposites onto paper. The solution bar coating paper were prepared at room temperature, under magnetic stirring, by dissolving 0.306 g powder of each sample in 6 mL of chloroform sonicated for 1 h. Each coating solution was then spread onto paper surface (10 × 10 cm, thickness 90 μm) mounted on a Teflon sheet using a glass spoon-shape bar and dried under ambient conditions (23 ± 2°C) for 24 h.

The compress hot melt coated paper was prepared in the following steps: 0.306 g powder of each sample was dispersed in 30 mL methanol and homogenized at 9000 rpm for 10 min using a homogenizer (Nissei AM-9, Japan). Then the nanocomposites polymer were spread onto paper (10 × 10 cm, thickness ca 90 μm) mounted on a Teflon sheet (10 × 10 cm) and dried overnight in an oven at 70°C. Finally, covered nanocomposite powder papers were placed between two Teflon sheets and inserted into a hydraulic hot press (Carver laboratory Press model 3925; Carver, Wabash, IN), heated to 190°C and subjected to a pressure of 1 bar for 2 min.

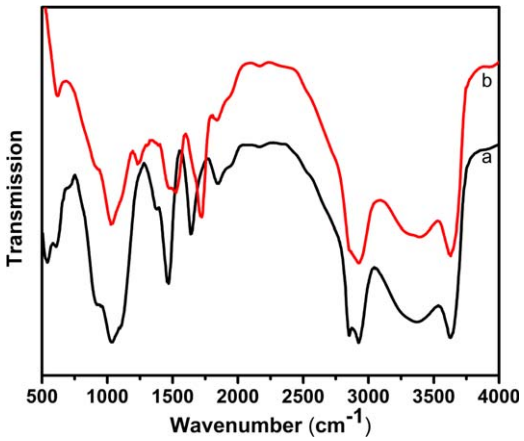

Figure 1. FTIR spectra of (a) CS30B and (b) M-CS30B. [Color figure can be viewed in the online issue, which is available at wileyonlinelibrary.com.]

RESULTS AND DISCUSSION

Analysis of the Chemical Structure of Surface Modified Clay

Fourier transform infrared (FTIR) spectra confirmed a reaction between the silanol hydroxyl groups of trisilanolisooctyl POSS® and hydroxyl groups of CS30B. Figure 1 shows the FTIR spectra of CS30B, and M-CS30B. Figure 1(a) (CS30B) exhibits a very broad band centered at 3629 cm^{-1} corresponding to the structural –OH groups in the clay sample. Assigned to the stretching vibration of the hydrogen-bond group, the absorptions at 2924 and 2852 cm^{-1} can be attributed to asymmetric and symmetric stretching vibrations of C–H bonds, whereas the absorption at 1469 cm^{-1} can be attributed to methylene bending vibrations, 1032 cm^{-1}. Also an intense broad band in the range of 1100–1000 cm^{-1}, can be readily assigned to the Si–O–R because of asymmetric Si–O–C stretching, these peaks are also noted in surface modified CS30B. In addition, Figure 1(b) exhibits the presence of a Si–CH2–R group indicated in 1231 cm^{-1}. A peak at 952 cm^{-1} confirms the presence of incompletely condensed Si-OH, 1028 cm^{-1} can be assigned to Si-O-Si originating from cage-structured POSS. The N-H bending vibrations observed at 1526 cm^{-1} and the strong peak at 1724 cm^{-1} confirmed the presence of cyclopentyl carbonyl-amine. The peak at 1473 cm^{-1} corresponded to the –CH2- scissoring and rocking modes. All these peaks provide strong evidence for the successful modification of CS30B with trisilanolisooctyl POSS®.

Morphologies of the PLA Nanocomposites

The clay minerals and the corresponding nanocomposites were analyzed by XRD in order to obtain information on the basal spacing and, any changes resulting from the processing. The interlayer distance (d-spacing) of clays inside the nanocomposites is obtained from Bragg's law:

$$2d \sin\theta = n\lambda_w \quad (2)$$

where d is the interlayer distance of clay, λ_w is the wavelength used, n is the order, which is equal to 1 for the first order, and θ is the measured angle.

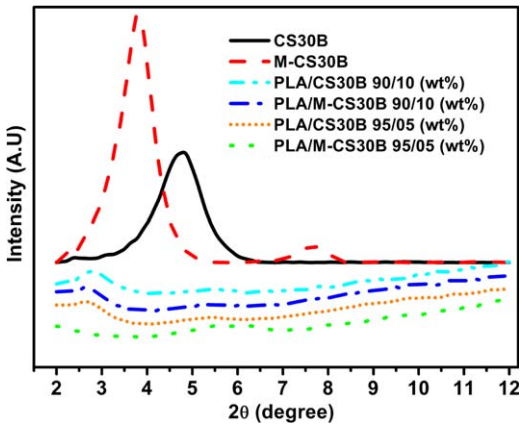

Figure 2. X-ray diffraction patterns of MMT and PLA nanocomposites. [Color figure can be viewed in the online issue, which is available at wileyonlinelibrary.com.]

XRD analyses of the CS30B and M-CS30B clay PLA/CS30B and PLA/M-CS30B nanocomposites are illustrated in Figure 2. After the grafting of trisilanollsooctyl POSS® onto CS30B, the *d* spacing for organo-modified clay initially presents at $2\theta = 4.8°$ (corresponding to a basal space of 1.82 nm), decreases to $2\theta = 3.8°$ which means *d* spacing is increased to 2.34 nm, thus indicating swelling of the nanoclay. The presence of second-order signals in the M-CS30B indicates a high degree of order in the modified clay mineral. Diffraction peaks were observed in the small angle region of the XRD patterns of PLA/CS30B and PLA/M-CS30B. At high nanoclay content (10 wt % clay), the shoulder centered on $2\theta = 3.0°$ and 2.6°, respectively. For PLA/CS30B with 5 wt % clay content, the shoulder centered on $2\theta = 2.8°$, which indicating that the dispersion is less accomplished in PLA/CS30B that PLA/M-CS30B nano-composite and partially intercalated structure with more aggregations of nanoclay may take place in the PLA matrix. This aggregation may impact the water vapor transmission rate because the aspect ratio of unmodified clay, which is a crucial factor for nanocomposites permeation properties in aggregated nanocomposite, is much lower than that of the intercalated or exfoliated nanocomposite. The aggregated clay may cause the formation of pores in the polymeric matrix, which potentially create preferential diffusion pathways for water vapor transport within the nanocomposite.[35–37]

The XRD pattern of the PLA/M-CS30B 95/05 wt/wt % sample shows no peak, which might be an indication of an exfoliated morphology or a disordered aggregate structure in the matrix.

In order to interpret the XRD observations, the phase behavior of the blends was studied using a TEM. The nanostructures revealed by the TEM (Figure 3) corresponded to the inferences drawn from XRD analysis and for confirming the formation of intercalated structures in polymer nanocomposites. The PLA/M-CS30B 95/05, PLA/M-CS30B 90/10, and PLA/CS30B 90/10 Nano-composites micrograph indicating the differences in the extent of intercalation and distribution of the clay layers.

In Figure 3(a), the TEM image shows that the clay is intercalated in the polymer matrix with the samples at 5 wt % M-CS30B loading, which creates a tortuous path for vapor molecules moving through the biopolymer matrix. The larger diffusion length leads to lower water vapor permeability.[38,39] On the other hand, as shown in Figure 3(c) with an increasing clay level, an increased degree of aggregation has also been seen for PLA/M-CS30B 90/10. The large particle aggregates were observed in TEM micrographs [Figure 3(c)], indicating that the CS30B particles are neither intercalated nor dispersed uniformly in the polymer matrix.

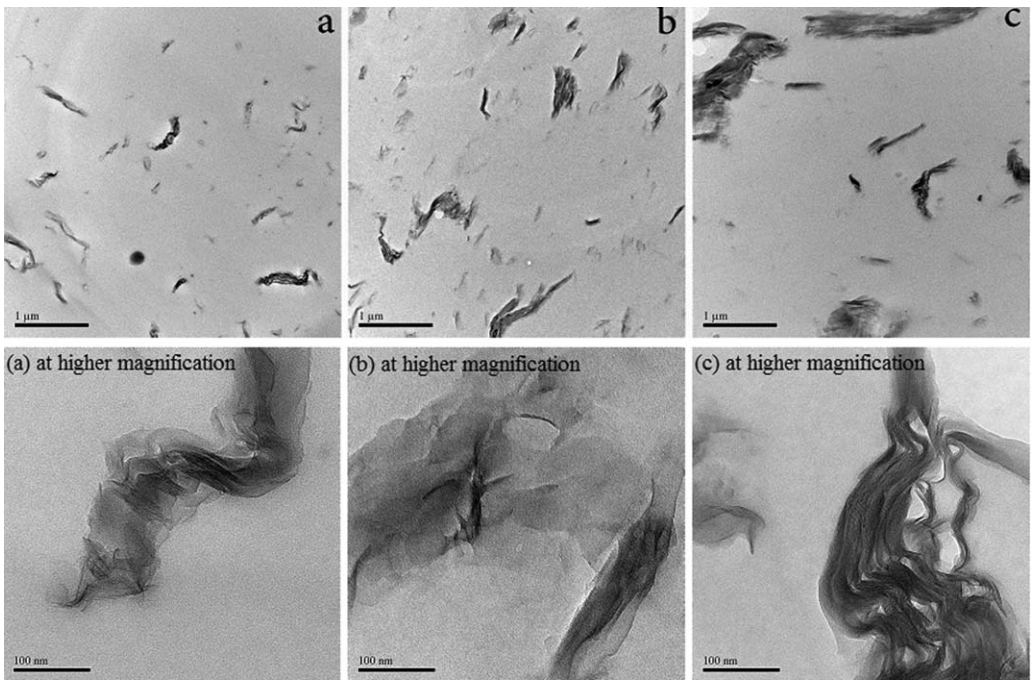

Figure 3. TEM images of PLA nanocomposites: (a) PLA/M-CS30B 95/05, (b) PLA/M-CS30B 90/10 and, (c) PLA/CS30B 90/10 at different magnification.

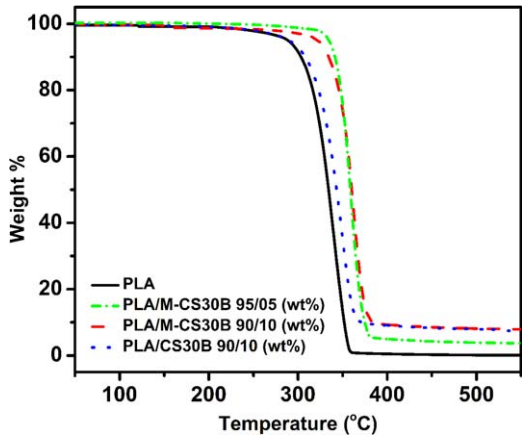

Figure 4. Weight loss for pure PLA and PLA nanocomposites. [Color figure can be viewed in the online issue, which is available at wileyonlinelibrary.com.]

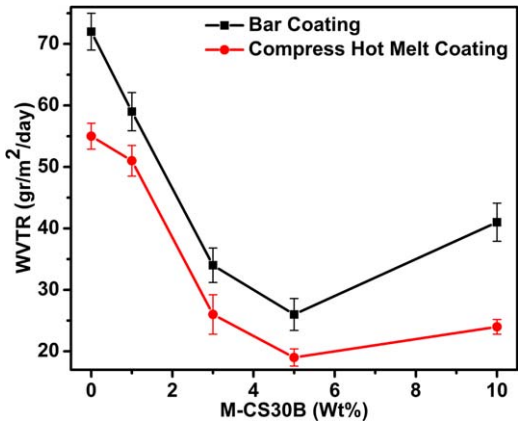

Figure 5. The WVTR of PLA/M-CS30B-coated paper with bar and compress hot melt coating methods. [Color figure can be viewed in the online issue, which is available at wileyonlinelibrary.com.]

Thermal decomposition of the PLA/Caly NanoComposites

TGA is a standard method of studying thermal decomposition of polymers. Figure 4 shows TGA thermogram PLA and PLA nanocomposites under N_2 atmosphere. All the samples show a large drop in the TGA curve. The TGA curves show that the onset of decomposition temperature of each nanocomposite sample is higher than that of pure PLA.

Onset and peak of degradation temperatures of the nanocomposites shift to higher temperatures. PLA/M-CS30B nanocomposites are more thermally stable than PLA/CS30B nanocomposites. The intercalated and homogeneous nanocomposite is the most thermally stable one among the samples. POSS itself is very thermally stable,[22] therefore, the MMT modified with POSS provides better thermal stability, compared to that of alkyl-ammonium modified MMTs. As a result, the MMT modified with POSS might diminish the application restriction of the organoclay in the engineering plastics, especially for those processed at high temperatures.

Table I. WVTR[a] Results of W&P Paper Bar-Coated and Compress Hot Melt Coated with PLA, PLA/CS30B, and PLA/M-CS30B Nano-Composites

Sample: wt/wt %	WVTR bar coated	WVTR Hot melt coated
W&P paper	300 ± 12	300 ± 12
PLA	72 ± 3.0	55 ± 2.1
PLA/CS30B 97/05	50 ± 3.5	35 ± 2.7
PLA/CS30B 90/10	67 ± 3.7	48 ± 2.9
PLA/M-CS30B 99/01	59 ± 3.1	51 ± 2.5
PLA/M-CS30B 97/03	34 ± 2.8	26 ± 3.2
PLA/M-CS30B 95/05	26 ± 2.6	19 ± 1.4
PLA/M-CS30B 90/10	41 ± 3.1	24 ± 1.2

[a] Test conditions: ΔRH 50% @ 23°C coat weight 25±2 g/m^2 and coat thickness 20 ± 2 μm.

The WVTR Measurement

Evaluated WVTR is defined as the steady water vapor flow over time through area of a body, normal to specific parallel surfaces, and under 50% relative humidity (ΔRH) at 23°C.

Water vapor transmission rate is a measure of the passage of water vapor through a substance. There are many industries where moisture control is critical. Moisture sensitive foods and pharmaceuticals are put in packaging with controlled WVTR to achieve the required quality, safety, and shelf life. Table I reveals variation in WVTR of PLA nanocomposites coated on writing paper with two different coating methods. As shown in Table I and Figure 5 by increasing the coated nanocomposites clay content from 0% to 5%, the WVTR value was reduced from 72 to 26 g/(m^2 day), because of the increase of the effective diffusion path length for the water vapor.[19,21,39]

By further increasing the clay content to 10%, the aggregated structure of MMT, as observed in TEM and XRD results, possibly provided channels or microvoids at the interface of polymer

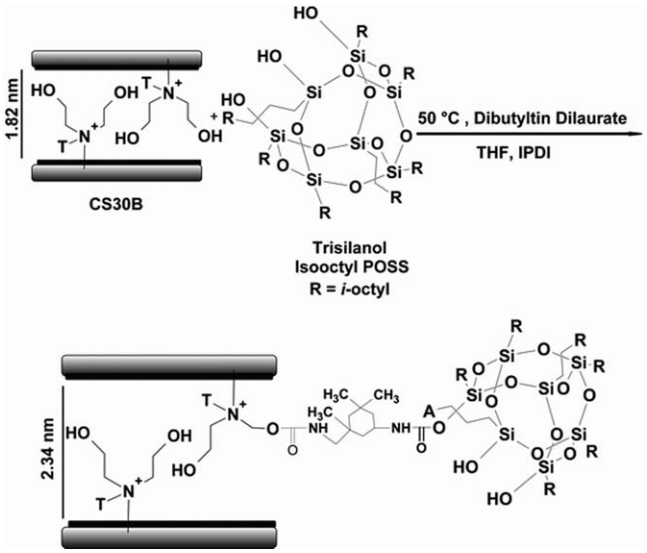

Scheme 2. Preparation of the Surface Modified Clays.

and clay.[35] As shown in Table I, the greater reduction in WVTR associated with M-CS30B might be attributed to the hydrophobic nature of trisilanolisooctyl POSS® and the higher *d* spacing of M-CS30B, which is also crucial for good dispersion of MMTs in the polymer matrix. Furthermore, Figure 5 shows that the WVTR of PLA/M-CS30B nanocomposite coated paper by compress hot melt method was significantly lower than that of the paper coated by bar coating method, regardless of M-CS30 content. This may be explained by the fact that more compact structure and smoother surface were formed through the compress hot melt coating method, thus creating the coating layer with less cracks and pores, particularly compared with those formed via dispersion (bar) coating method.[14]

CONCLUSIONS

This study clearly demonstrated that the incorporation of Cloisite® 30B MMT clay and the Cloisite® 30B clay modified with POSS, either via a solution blending process or paper coating using bar coating and hot press coating methods, improved the water vapor barrier properties of coated paper significantly. The paper coated with binary and ternary nanocomposites diminishes the water vapor transmission rate by 74% [26 g/(m^2 day)], as compared to the paper coated with pure PLA. The dispersion or phase behavior of the M-CS30B in PLA matrix was revealed by XRD. The interclation of clay with PLA was further demonstrated using TEM. Overall, the hot press coating method is an effective approach in improving the water vapor resistance of the coated papers.

ACKNOWLEDGMENTS

Authors are grateful to NSERC Strategic Network—Innovative Green Wood Fibre Product (Canada) for funding and NSF China (No. 51379077).

REFERENCES

1. Spinner, J., *Packaging Digest 49*, 26, **2012**.
2. Aulin, C.; Gällstedt, M.; Lindström, T. *Cellulose 17*, 559, **2010**.
3. Rhim, J. W.; Kim, J. H. *J. Food Sci. 74*, E105, **2009**.
4. Paper and Paperboard Packaging Technology; Blackwell Publishing Ltd, **2007**; Chapter 1, pp 1–49.
5. Xue, M.; Wang, S. In Adv. Mater. Res., Proceedings of the International Conference on Chemical, Material and Metallurgical Engineering, ICCMME 2011, Beihai, China, December 23–25, **2011**.
6. Fehr, B. A.; Domenech, A.; Zuercher, C. In TAPPI Eur. PLACE Conf., Proceedings of the 12th European PLACE Conference, Budapest, Hungary, May 18–20, **2009**.
7. Furuheim, K. M.; Axelson, D. E.; Antonsen, H. W.; Helle, T. *J. Appl. Polym. Sci. 91*, 218, **2004**.
8. Tuominen, M.; Ek, M.; Saloranta, P.; Toivakka, M.; Kuusipalo, J., *Packag. Technol. Sci.* **2013**, *26*, 201.
9. Lahti, J.; Tuominen, M.; Penttinen, T.; Rasanen, J. P.; Kuusipalo, J. In TAPPI Eur. PLACE Conf., Proceedings of the 12th European PLACE Conference, Budapest, Hungary, May 18–20, **2009**.
10. Colomines, G.; Ducruet, V.; Courgneau, Ć.; Guinault, A.; Domenek, S. *Polym. Int. 59*, 818, **2010**.
11. Lahtinen, K.; Kotkamo, S.; Koskinen, T.; Auvinen, S.; Kuusipalo, J. *Packag. Technol. Sci. 22*, 451, **2009**.
12. Auras, R.; Harte, B.; Selke, S. *J. Appl. Polym. Sci. 92*, 1790, **2004**.
13. Rhim, J. W.; Hong, S. I.; Ha, C. S. *LWT Food Sci. Technol. 42*, 612, **2009**.
14. Rhim, J. W. *Food Sci. Biotechnol. 18*, 1155, **2009**.
15. Tarameshlou, M.; Jafari, S. H.; Khonakdar, H. A.; Fakhravar, A.; Farmahini-Farahani, M. *Iran. Polym. J. (English Edition) 19*, 521, **2010**.
16. Tarameshlou, M.; Jafari, S. H.; Khonakdar, H. A.; Farmahini-Farahani, M.; Ahmadian, S. *Polym. Compos. 28*, 733, **2007**.
17. Amass, W.; Amass, A.; Tighe, B. *Polym. Int. 47*, 89, **1998**.
18. Bordes, P.; Pollet, E.; Avérous, L. *Prog. Polym. Sci. (Oxford) 34*, 125, **2009**.
19. Silvestre, C.; Duraccio, D.; Cimmino, S. *Prog. Polym. Sci. (Oxford) 36*, 1766, **2011**.
20. Chiu, C. W.; Lin, J. J. *Prog. Polym. Sci. (Oxford) 37*, 406, **2012**.
21. Duncan, T. V. *J. Colloid Interface Sci. 363*, 1, **2011**.
22. Wu, J.; Mather, P. T. *Polym. Rev. 49*, 25, **2009**.
23. Lee, J. H.; Jeong, Y. G. *J. Appl. Polym. Sci. 115*, 1039, **2010**.
24. Jiang, B.; Tao, W.; Lu, X.; Liu, Y.; Jin, H.; Pang, Y.; Sun, X.; Yan, D.; Zhou, Y. *Macromol. Rapid Commun. 33*, 767, **2012**.
25. Silva, R.; Salles, C.; Mauler, R.; Oliveira, R. *Polym. Int. 59*, 1221, **2010**.
26. Chen, S.; Hu, J. *Polym. Int. 61*, 314, **2012**.
27. Hossain, M. D.; Yoo, Y.; Lim, K. T. *J. Appl. Polym. Sci. 119*, 936, **2011**.
28. Lee, J. H.; Jeong, Y. G. *Fibers Polym. 12*, 180, **2011**.
29. Kanezashi, M.; Shioda, T.; Gunji, T.; Tsuru, T. *AIChE J. 58*, 1733, **2012**.
30. Hao, N.; Böhning, M.; Schönhals, A. *Macromolecules 43*, 9417, **2010**.
31. Song, J.; Zhao, J.; Ding, Y.; Chen, G.; Sun, X.; Sun, D.; Li, Q. *J. Appl. Polym. Sci. 124*, 3334, **2012**.
32. Li, Y. C.; Mannen, S.; Schulz, J.; Grunlan, J. C. *J. Mater. Chem. 21*, 3060, **2011**.
33. Zhang, X.; Yan, C.; Fang, S.; Zhang, C.; Jia, T.; Zhang, Y. *J. Polym. Res. 17*, 631, **2010**.
34. Pan, H.; Qiu, Z. *Macromolecules 43*, 1499, **2010**.
35. Tang, X.; Alavi, S. *J. Agric. Food Chem. 60*, 1954, **2012**.
36. Choudalakis, G.; Gotsis, A. D. *Eur. Polym. J. 45*, 967, **2009**.
37. Nazarenko, S.; Meneghetti, P.; Julmon, P.; Olson, B. G.; Qutubuddin, S. *J. Polym. Sci. B Polym. Phys. 45*, 1733, **2007**.
38. Bordes, P.; Pollet, E.; Avérous, L. *Prog. Polym. Sci. 34*, 125, **2009**.
39. Chiu, C.-W.; Lin, J.-J. *Prog. Polym. Sci. 37*, 406, **2012**.